sensors

MDPI

Article

60–700 K CTAT and PTAT Temperature Sensors with 4H-SiC Schottky Diodes

Razvan Pascu [1,2,3,*], Gheorghe Pristavu [2], Gheorghe Brezeanu [2], Florin Draghici [2], Philippe Godignon [4], Cosmin Romanitan [1], Matei Serbanescu [2] and Adrian Tulbure [5]

1 National Institute for Research and Development in Microtechnologies—IMT Bucharest, 126A, Erou Iancu Nicolae Street, 077190 Bucharest, Romania; cosmin.romanitan@imt.ro
2 Faculty of Electronics, Telecommunications and Information Technology, University "Politehnica" of Bucharest, 060042 Bucharest, Romania; gheorghe.pristavu@upb.ro (G.P.); gheorghe.brezeanu@dce.pub.ro (G.B.); florin.draghici@upb.ro (F.D.); matei.serbanescu@stud.etti.upb.ro (M.S.)
3 Romanian Young Academy, Research Institute of the University of Bucharest, University of Bucharest, 030018 Bucharest, Romania
4 Centre Nacional de Microelectrònica, CNM-CSIC, 08193 Barcelona, Spain; philippe.godignon@cnm.es
5 Department of Informatics, Mathematics and Electronics, Faculty of Exact Sciences and Engineering, University "1 Decembrie 1918" of Alba Iulia, No. 5, Gabriel Bethlen Street, 510009 Alba Iulia, Romania; aditulbure@uab.ro
* Correspondence: razvan.pascu@imt.ro

Abstract: A SiC Schottky dual-diode temperature-sensing element, suitable for both complementary variation of V_F with absolute temperature (CTAT) and differential proportional to absolute temperature (PTAT) sensors, is demonstrated over 60–700 K, currently the widest range reported. The structure's layout places the two identical diodes in close, symmetrical proximity. A stable and high-barrier Schottky contact based on Ni, annealed at 750 °C, is used. XRD analysis evinced the even distribution of Ni_2Si over the entire Schottky contact area. Forward measurements in the 60–700 K range indicate nearly identical characteristics for the dual-diodes, with only minor inhomogeneity. Our parallel diode (*p-diode*) model is used to parameterize experimental curves and evaluate sensing performances over this far-reaching domain. High sensitivity, upwards of 2.32 mV/K, is obtained, with satisfactory linearity (R^2 reaching 99.80%) for the CTAT sensor, even down to 60 K. The PTAT differential version boasts increased linearity, up to 99.95%. The lower sensitivity is, in this case, compensated by using a high-performing, low-cost readout circuit, leading to a peak 14.91 mV/K, without influencing linearity.

Keywords: wide-range temperature sensor; SiC-Schottky diode; sensitivity; linearity; readout circuit

Citation: Pascu, R.; Pristavu, G.; Brezeanu, G.; Draghici, F.; Godignon, P.; Romanitan, C.; Serbanescu, M.; Tulbure, A. 60–700 K CTAT and PTAT Temperature Sensors with 4H-SiC Schottky Diodes. *Sensors* **2021**, *21*, 942. https://doi.org/10.3390/s21030942

Academic Editor: Arunas Ramanavicius

Received: 29 December 2020
Accepted: 28 January 2021
Published: 31 January 2021

Publisher's Note: MDPI stays neutral with regard to jurisdictional claims in published maps and institutional affiliations.

Copyright: © 2021 by the authors. Licensee MDPI, Basel, Switzerland. This article is an open access article distributed under the terms and conditions of the Creative Commons Attribution (CC BY) license (https://creativecommons.org/licenses/by/4.0/).

1. Introduction

Space missions, automotive, and various industries involve applications with a wide thermal variation and a large temperature range for detection. Here, temperature sensing plays a major role in ensuring safe operation or quality control capabilities. However, when working in such hostile environments, the performances of conventional sensing solutions can be affected by accuracy degradation or worse, general failure [1,2]. Usually, these detection systems include a series of commercial temperature sensors, which are based on thermocouples [3] or resistive temperature detectors [4,5]. Their accuracy and reliability are comparable, but neither are competitive with semiconductor-based temperature sensors [6,7], especially those fabricated on robust materials [8–10]. The increased request for high temperature-capable applications makes research in this domain constantly strive to find alternative solutions, which can satisfy specifications. However, electronic devices and systems based on conventional semiconductors, such as Si, are limited to operate at temperatures below 400 K [11]. On the other hand, wide-bandgap semiconductors have

attracted much attention due to their electrical properties, together with their superior mechanical and chemical resilience. In particular, silicon carbide (SiC) has emerged as a viable alternative to replace Si in power and harsh-environment applications. SiC technology is very similar with that of Si and, in the last decade, its manufacturing processes have matured considerably, especially regarding the improvement in fabricated material defect density [12–18] and reliability of SiC-based devices [19–26]. In this regard, the simplest and most technologically mature device is the Schottky diode (SBD). When working as a temperature sensor [27], the key performances are linearity of the voltage-temperature dependence and long-term stability. The Schottky metal is also crucial, as the resulting contact's barrier height (SBH) needs to be sufficient in order to ensure exponential current-voltage dependence for the forward characteristics over several orders of magnitude, at all temperatures of interest. In this sense, many literature contributions report metals such as Ti/Al [28], Ni [29], Pt [30] being used to achieve stable Schottky contacts on SiC. The most promising candidate for high temperature SiC Schottky diode-based sensors is Ni, due to its high work function and the capability to form very stable nickel silicide compounds on SiC after rapid post-metallization annealing in inert atmospheres [31]. It ensures a reasonably constant SBH, with values upwards of 1.73 V, for wide temperature ranges [25]. However, because of the detrimental effect of Schottky contact inhomogeneity [25,32–38], these indicators of merit degrade significantly for large temperature variations. As such, there are no reports of SiC-Schottky diodes working predictably over vast temperature ranges, much less so sensors. However, with the proposal of differential measurement techniques for SiC-Schottky diode temperature sensors [28,39], which considerably increase sensing linearity, as well as the recent introduction of a practical inhomogeneity modeling technique [40], the premises are set for investigating the potential performances of these devices over ranges spanning from cryogenic levels to high-temperature domains.

In this paper, we present wide-temperature sensing performances of a dual Schottky diode structure capable of working in either single or differential configurations. The structure is designed to operate at temperatures in the 60–700 K range. In order to increase sensitivity while maintaining linearity levels at an optimum, a simple and cost-effective readout circuit architecture is proposed and simulated for the differential topology.

2. Materials and Methods

2.1. Temperature Detection Methods Based on SiC Schottky Diodes

The forward voltage of Schottky diodes, biased at constant current, is given by the thermionic emission equation (neglecting the impact of the series resistance) [8,25]:

$$V_F \approx n\Phi_{Bn,T} + nV_{th} \ln\left(\frac{I_F}{A_n A_S T^2}\right) \tag{1}$$

where A_n is Richardson's constant, A_S is the contact area, V_{th} is the thermal voltage, n is the ideality factor, and $\Phi_{Bn,T}$ is the conventional barrier. From Equation (1), a quasi-linear complementary variation of V_F with absolute temperature (CTAT) can be expressed, in respect to a reference (T_0), thus:

$$V_F(T) = n\Phi_{Bn,T} - \left[n\Phi_{Bn,T} + 2nV_{th0} \ln\left(\frac{T}{T_0}\right) - V_F(T_0)\right]\frac{T}{T_0} \tag{2}$$

V_{th0} is the thermal voltage associated with T_0. From Equation (2), using Schottky diodes as CTAT sensors over moderate domains yields high sensitivities (in excess of 2 mV/K, depending on bias current levels, which determine $V_F(T_0)$) and reasonable linearity [24,28], while using simple and cost-effective readout circuits [8]. However, extending the operating temperature range evinces two significant causes for linearity degradation and sensitivity inconsistency:

I. The innate variation of V_F. Equation (2) contains a non-linearly temperature-dependent logarithmic term, which becomes significant when extending the T domain.

II. Contact inhomogeneity. Analyzing Equation (2), it can be seen that Schottky diodes used for temperature sensing need to have constant barrier height and ideality factor values over the entire range of interest. Fluctuations in these parameters, primarily due to Schottky contact inhomogeneity, have been, however, ubiquitously reported [36,41–45]. The domain of variation for n and $\Phi_{Bn,T}$ is proportional with temperature range.

These sources of performance degradation can be mitigated using sensing methods based on differential forward voltage (ΔV_F) [39,46]. In contrast to the standard technique, ΔV_F can either increase (PTAT) or decrease (CTAT) with absolute temperature. Three ways of obtaining ΔV_F are discussed:

The single diode, dual current levels (SDDC) approach utilizes the voltage differential from a single diode, biased sequentially at two current levels, $I_{Fh} > I_{Fl}$ (for the PTAT case):

$$\Delta V_F(T) = V_{Fh} - V_{Fl} \overset{(1)}{\Rightarrow} \Delta V_F(T) = n \cdot V_{th} \cdot \ln\left(\frac{I_{Fh}}{I_{Fl}}\right) = n \cdot \frac{k}{q} \cdot T \cdot \ln\left(\frac{I_{Fh}}{I_{Fl}}\right) \tag{3}$$

This expression for $\Delta V_F(T)$ is directly proportional with temperature. The impact of contact inhomogeneity can also be alleviated by carefully tuning the I_{Fh} and I_{Fl} levels. Thus, SDDC is the technique that ensures best linearity. Sensitivity magnitude is proportional to the I_{Fh}/I_{Fl} ratio. The downside is that the sequential biasing involves a readout circuit with a significantly more complex control loop. Acquiring the differential voltage requires either digital memory blocks or sample-and-hold cells, thereby delaying signal processing and increasing response times.

For the dual diode, single current level (DDSC) approach, the voltage difference is obtained from two diodes with different active areas ($A_{Sh} > A_{Sl}$), biased at the same current:

$$\Delta V_F = V_{Fh} - V_{Fl} \overset{(1)}{\Rightarrow} \Delta V_F(T) = n \cdot V_{th} \cdot \ln\left(\frac{A_{Seffh}}{A_{Seffl}}\right) \tag{4}$$

This technique needs both diodes to have identical, temperature-invariable n and $\Phi_{Bn,T}$. In Equation (4), it is mandatory to use the effective contact areas ($A_{Seffh,l}$), which generally differ greatly from their nominal values ($A_{Sh,l}$). We presented procedures to evaluate A_{Seff} for Schottky diodes with non-uniform contacts (like Ni/SiC) [25,40]. While this technique requires readout circuits which are comparable in complexity and cost with the standard temperature detection method, its performances are much more susceptible to the quality of the Schottky interface. Inhomogeneities present on the contact surface, for either or both diodes, can significantly increase local current flow, leading to apparent effective area modifications, which then affect linearity and sensitivity consistency.

Finally, the dual diode, dual current levels (DDDC) approach finds a suitable compromise between the previous techniques by employing two identically-sized diodes, each biased at a different current. In this case, the differential voltage expression is identical to Equation (3). This method inherits the SDDC technique's robustness to contact inhomogeneity influence through tuning of I_{Fh} and I_{Fl} values, while also allowing for the use of a simple and cost-effective readout circuit architecture. Sensor system performances are only noticeably affected by mismatches between either the dual diodes or their bias current sources.

Considering the advantages and drawbacks of the aforementioned temperature detection techniques, the DDDC method (with PTAT variation) was selected for implementation and comparison with the standard approach (single diode, biased at constant current, CTAT dependence), in the context of temperature sensing in a very wide range.

2.2. Sample Preparation

The sensor structures consist of two SiC Schottky devices placed in close proximity (dual-diodes), with diagonal reverse symmetry, as is evinced in the Figure 1.

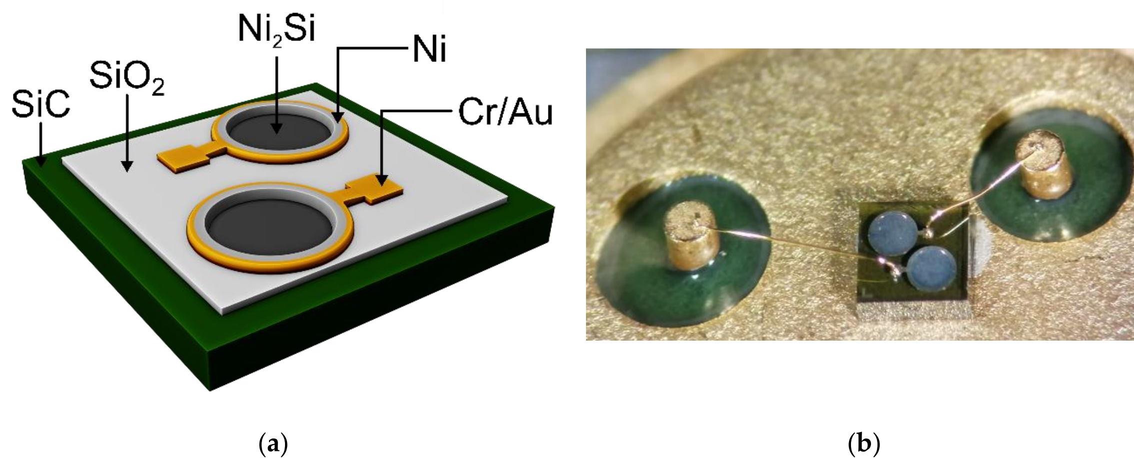

(a) (b)

Figure 1. Dual-diode sensing element: (**a**) schematic illustration and (**b**) encapsulated structure.

The fabrication process started from an n-type 4H-SiC substrate with 8 μm epitaxial layer, having~10^{16} cm^{-3} doping concentration. After a standard RCA [47] chemical cleaning, an initial dense layer of SiO_2 (500 nm) was grown by Low Pressure Chemical Vapor Deposition (LPCVD), followed by a thermal annealing in O_2 atmosphere at a temperature of 950 °C, for 30 min. Another SiO_2 layer was subsequently deposited, without annealing, resulting in a less compact film. Next, circular active windows, with 400 μm diameters, were etched (using NH_4F/CH_3-COOH (180 mL/200 mL) solution in the oxide layers, resulting in a ramp profile termination [8,10]. This oxide ramp ensures a smooth current density distribution. After the active areas defining, the ohmic contact on the backside was obtained by deposition of a thin film of Ni (100 nm), followed by a rapid post-metallization annealing at a temperature of 1050 °C for 3 min in Ar atmosphere. Another thin film deposition of Ni (100 nm), in the active windows, was performed. A rapid post-metallization annealing at a temperature of 750 °C for 3 min in Ar atmosphere was carried out in order to obtain the Schottky contacts. Contact pads and the final back contact were finally defined after a deposition of (Cr (20 nm)/Au (300 nm)) on both sides of wafers. The test structures were diced into dual-diode chips and encapsulated in compact TO-39 packages using wire-bonding technology, as shown in Figure 1b.

2.3. Readout Circuit Architecture

The readout circuit is used to acquire and amplify the forward voltage difference given by the aforementioned dual-diode sensing element. It also biases the two identical diodes at different constant currents (the DDDC approach). Figure 2 represents the schematic of the proposed circuit. It includes a cost-effective, top-linearity instrumentation amplifier, comprising two low-noise, high-reliability OP07 [48] operational amplifiers, four resistors, and a potentiometer (P_1-Figure 2) for output span tuning. The dual SiC Schottky diode structure is biased by an *I:nI Bias* block, based on the high-precision REF200 [49] current reference produced by Texas Instruments.

In order to greatly simplify the transfer function of the instrumentation amplifier, $R_1 = R_2$ and $R_3 = R_4$ is usually considered:

$$V_O = \left(1 + \frac{R_3}{R_1} + 2\cdot\frac{R_3}{P_1}\right)\cdot(V_{Fh} - V_{Fl}) \tag{5}$$

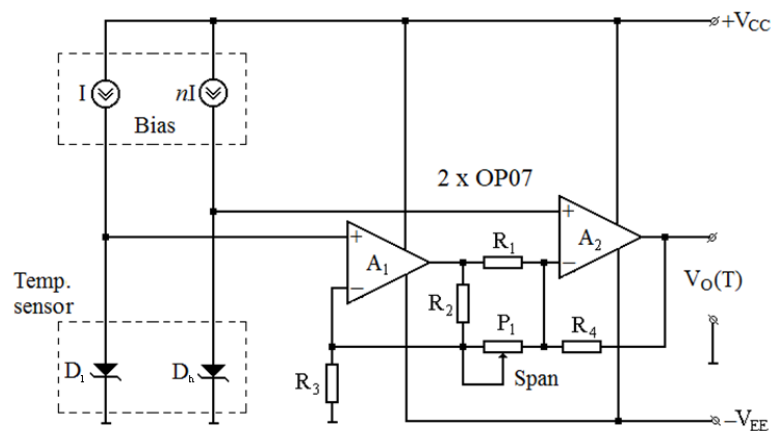

Figure 2. Schematic of the differential temperature measurement circuit.

For an optimum common-mode rejection, all resistors ($R_{1–4}$) should be equal. As a result:

$$V_O = 2 \cdot \left(1 + \frac{R_1}{P_1}\right) \cdot (V_{Fh} - V_{Fl}) \tag{6}$$

The value of 10 kΩ was selected for these components in order to obtain a suitable compromise between power consumption, phase margin, and thermal noise. Because sensing diode voltages can reach low values at high operation temperatures, the circuit is powered by a ±15 V supply, which ensures good linearity over the entire output swing. This is the only noticeable difference between this topology, suitable for differential PTAT sensing, and the one described in [8], used for CTAT sensors. Otherwise, the two readout circuits are similar in complexity, cost, and gain tuning flexibility, offering high versatility over a wide array of temperature monitoring applications.

3. Results

3.1. X-ray Diffraction Analysis

In order to preliminarily assess the Schottky and ohmic contacts' homogeneity, X-ray diffraction measurements were performed in grazing incidence geometry. The X-ray source was kept at 0.5°, while the detector scanned from 2θ = 20° up to 70°. A scan step of 0.01° at 4°/min was used for these investigations. Figure 3 presents the Grazing Incidence X-ray Diffraction (GI-XRD) patterns for both contacts.

As can be observed in Figure 3, both contacts present multiple diffraction peaks. These were assigned unambiguously as the Ni_2Si phase, according to International Center for Diffraction Data (ICDD) database with card no. 900–9210 that belongs to the orthorhombic 62: Pbnm spatial group. Thus, the thermal treatment led to the formation of only the Ni_2Si phase, without any additional phases. La Via et al. [50] report that a reaction between Ni and Si gives only the formation of the Ni_2Si phase over a large annealing temperature range, between 600 °C and 950 °C. Later, the existence of a combination between $Ni_{31}Si_{12}$ and Ni_2Si phases at 600 °C with an increase in Ni_2Si percentage at 950 °C was also observed by XRD [51]. Kuchuk et al. [52] reported the formation of the Ni_2Si phase as a result of a thermal treatment at 600 °C for 15 min. Increasing the annealing temperature further improved the occurrence rate of the $NiSi_2$ phase. In our X-ray patterns, there are no traces of Ni or Si peaks, indicating that the thermally activated interaction between Ni and SiC had occurred. Moreover, taking into account the large area of the X-ray spot, namely 1 cm^2, we conclude that there is no residual Ni on either contact. Regarding the crystal quality, the diffraction peak position of the Schottky contact, indicated with blue dashed line in Figure 3, was attributed to different Miller indices. There is a preferential orientation along the (311) direction. The increase in annealing temperature led to more pronounced polycrystalline features for the ohmic contact, which does not present a clear preferential orientation. The mean crystalline size was evaluated from a Williamson-Hall plot [53], with

values of 20.1 nm (Schottky contact) and 19.6 nm (ohmic contact). Comparable crystalline domain sizes indicate that the thermal treatment did not induce the formation of additional structural defects. The XRD findings suggest that the thermal treatment led to Ni_2Si phase formation on the entire Schottky and ohmic contact areas, for each of the dual-diodes. Additional dislocations were not generated.

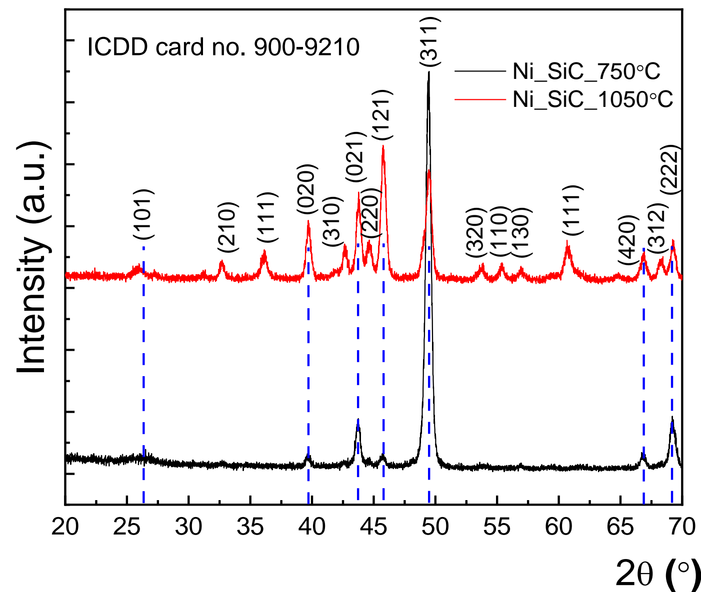

Figure 3. Grazing Incidence X-ray Diffraction (GI-XRD) patterns for the Schottky contact annealed at 750° (black line) and for the ohmic contact annealed at 1050 °C (red line), respectively. The dashed lines indicate the diffraction peaks position of the Schottky contact besides to the ohmic one.

3.2. Modeling and Sensing Performances

The test samples were electrically characterized over a wide range of temperatures, starting from 60 K up to 700 K, with a step of 20 K. A Keithley 4200 Semiconductor Characterization System coupled with a Janis closed cycle refrigerator (CCS-450), capable of providing adequate means of cooling samples to temperatures below 77 K (liquid nitrogen), was used to perform measurements from 60 K to 500 K. For high-temperature measurements (300–700 K), the system described in [8] was used, comprising a Varian Chromatograph Oven and another Keithley 4200 SCS. Current-voltage (I-V) characteristics were acquired with the two systems on different days and experimental results were compared in the common 300–500 K interval to ensure reproducibility. The high-temperature stability of structures obtained with similar technological processes was demonstrated by thermal-cycling in [8]. Figure 4 depicts exemplary I-V-T characteristics for the dual diodes (D_A and D_B). It can be seen that the devices have nearly identical forward electrical behavior over the entire 60–700 K domain. The exponential portion of the curves can be identified for each experimental characteristic, spanning at least five orders of magnitude, even at 700 K. For these reasons, it was considered that D_A and D_B both have the same Schottky contact parameters.

For the curves in Figure 4, the conventional barrier and ideality factor were extracted at each temperature, using the conventional method [54]. $\Phi_{Bn,T}$ was found to increase with temperature from 0.94 V to approx. 1.7 V, while n decreased from 1.85 to 1.01. These results indicate the presence of contact surface inhomogeneity. Thus, our recently introduced parallel-diode (*p-diode)* model was used in order to thoroughly characterize the sample, according to [40]:

$$I_F = \sum_{i=1}^{m} I_{F,i} = A_n A_S T^2 \sum_{i=1}^{m} \exp\left(\frac{-\Phi_{Bn,i}}{V_{th}} - p_{eff,i}\right)\left[\exp\left(\frac{V_F - R_{S,i} I_{F,i}}{n V_{th}}\right) - 1\right] \quad (7)$$

The model assumes that an inhomogeneous contact comprises multiple regions which behave like ideal, parallel-connected diodes, each with associated barrier height ($\Phi_{Bn,i}$), non-uniformity parameter ($p_{eff,i}$), near-unity ideality factor ($n \cong 1$), and series resistance ($R_{S,i}$). Out of the entire number of regions, only a few (counted by the model parameter *m*) contribute significantly to current conduction over the entire investigated temperature range. The p_{eff} value is used to estimate the surface area for each of these essential regions [25,40]. Note that the total area occupied by the *m* regions can only be equal to or less than the nominal area (A_S), with closer values indicating a better-quality diode.

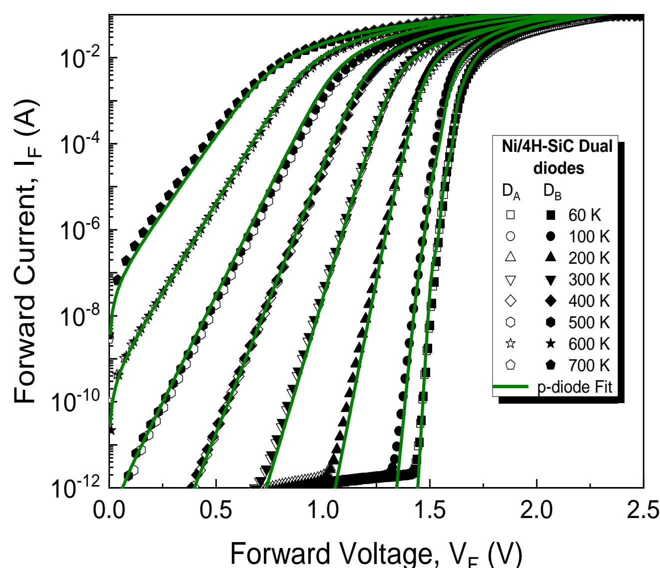

Figure 4. Forward I-V characteristic for the dual SiC Schottky diodes. Measurement data (symbols) and their p-diode model-fitted counterparts (lines).

In order to fully replicate the characteristics in Figure 4, *m* = 4 parallel-connected diodes (Dp1–Dp4) were necessary, with their model-parameters given in Table 1. Φ_{Bn} values are constant throughout the entire temperature range and tend towards the theoretical barrier height value for Ni_2Si [25].

Table 1. Fitting parameters for sample S1.

Parallel Diode	Φ_{Bn} [V]	p_{eff}	n
Dp1	1.56	8.75	1.01
Dp2	1.615	4.14	
Dp3	1.665	1.84	
Dp4	1.73	0.23	

The values of p_{eff} (Table 1) were estimated using Richardson plots over various temperature intervals and iteratively tuned, according to the technique proposed in [25,40]. Afterwards, they were used to determine occupied area percentages in respect to A_S, for each parallel diode, as depicted in Figure 5. Note that nearly the entire Schottky contact surface is used for current conduction, especially at high bias and high temperatures.

Our model entails the evaluation of series resistance contributions [40]. Accordingly, the variations with temperature for the parallel diodes' series resistances are illustrated in Figure 6. Because Dp3 and Dp4 have comparable current contributions at all temperatures, their individual series resistances could not be deconvoluted. Their combined ohmic behavior was determined, at each temperature, with Cheung's method [54]. R_S values for Dp1 and Dp2 were adjusted to account for area differences, while keeping the same variation trend as $R_{S,Dp3} \,||\, R_{S,Dp4}$.

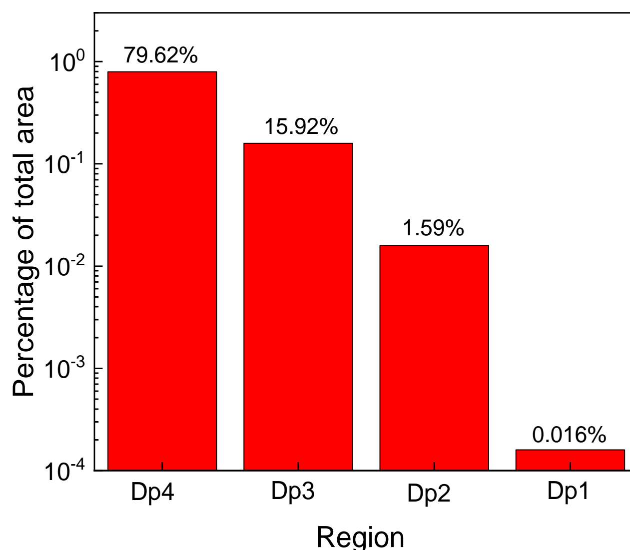

Figure 5. Parallel diode area percentages in respect to total Schottky contact area.

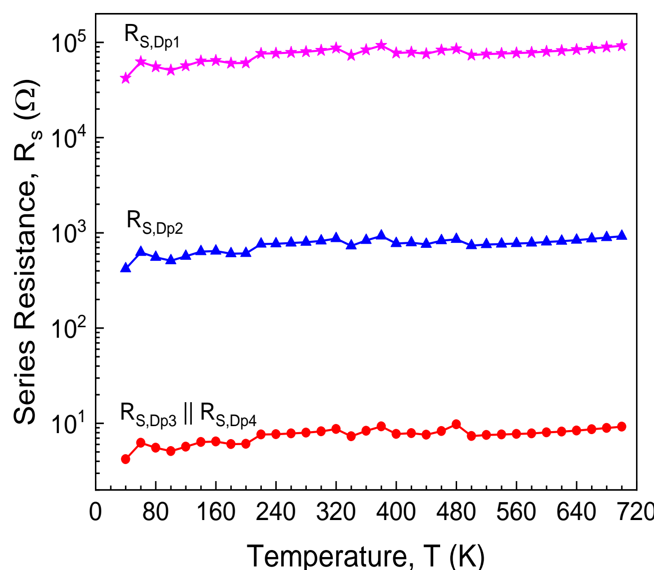

Figure 6. Series resistance temperature variation for the model parallel diodes (Dp1–Dp4).

The model-fitted forward curves, also depicted in Figure 4 (lines), are in good agreement with measurements for the entire temperature span. The fitting used Equation (7) with m = 4, the parameters from Table 1, and R_S data from Figure 6. Notably, the ideality factor, n = 1.01, was considered for each parallel diode, in the full 60–700 K domain. Dp3 and Dp4 significantly affect total current at all temperatures, especially in the high-bias region. Dp1 and Dp2 only influence conduction in the low-bias, low-temperature portion of the forward characteristics. Their impact becomes negligible past 200 K. For this investigated sample, our model [40] was able to completely reflect experimental forward behavior even at cryogenic temperatures (Figure 4). This is because, due to their area sizes which add up to almost the entire nominal surface (Figure 5), none of the parallel diodes suffers from the "pinch-off" effect [41]. This result attests to the high uniformity of the Schottky metal (Ni_2Si, see Figure 3).

Analyzing the modeled electrical behavior of the dual-diodes (Figures 4–6 and Table 1), a few conclusions can be drawn about their usability as temperature sensors:

I. D_A and D_B may work over the entire domain of 60–700K, due to the localized effects of the parallel diodes. Forward bias-current values can be tuned to higher

levels in order to restrict inhomogeneity influences (having only two parallel diodes dictate the majority current flow, rather than all of them).

II. The standard CTAT sensing technique (using a single diode, either D_A or D_B, biased at constant current) will suffer from poor linearity. This is because both Dp3 and Dp4 significantly affect conduction in the high-bias domain, but with different contributions depending on temperature.

III. Using PTAT sensing techniques based on voltage difference can greatly improve linearity. As Dp3 and Dp4 have comparable barrier heights and effective areas, their combined apparent barrier height will have a slow temperature variation, which will be mitigated by forward voltage differentiation.

Following these conclusions, an assessment of D_A and D_B temperature sensing performances was carried out. Their forward voltage variations with temperature, at different constant current levels, are presented in Figure 7, for each diode.

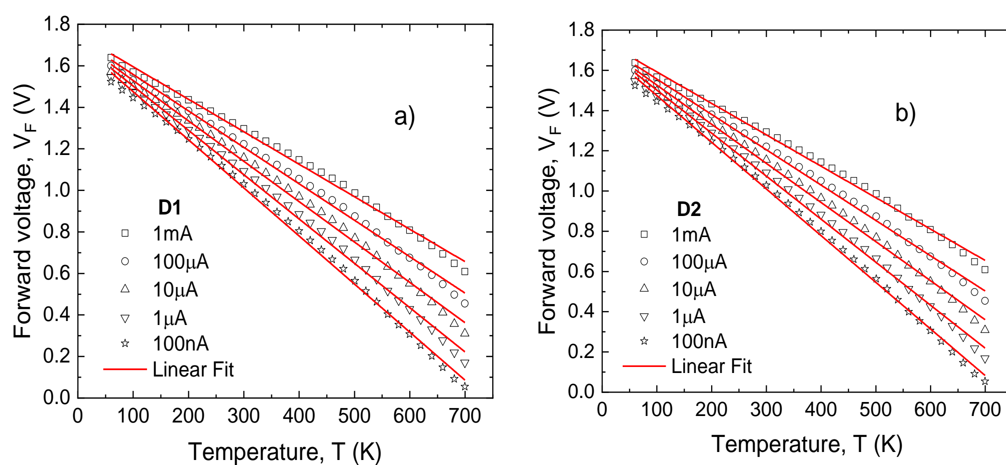

Figure 7. Forward voltage as a function of temperature for (**a**) D_A and (**b**) D_B at several bias currents.

As expected, a CTAT dependence is obtained. For each individual device, a linear regression process on the characteristics in Figure 7 was performed. The slope of the fitted curves yielded the sensitivity. In order to assess linearity, the adjusted coefficient of determination (R^2) was also determined. This parameter quantitatively evaluates how well a proposed model (in this case, a linear dependence) predicts experimental measurements. Additionally, for each current level, the fitting root mean squared error was divided by associated sensitivity in order to determine the temperature error (*e*T) [55]. As expected, *e*T varies complementarily to R^2 [55]. Results are presented in Figure 8.

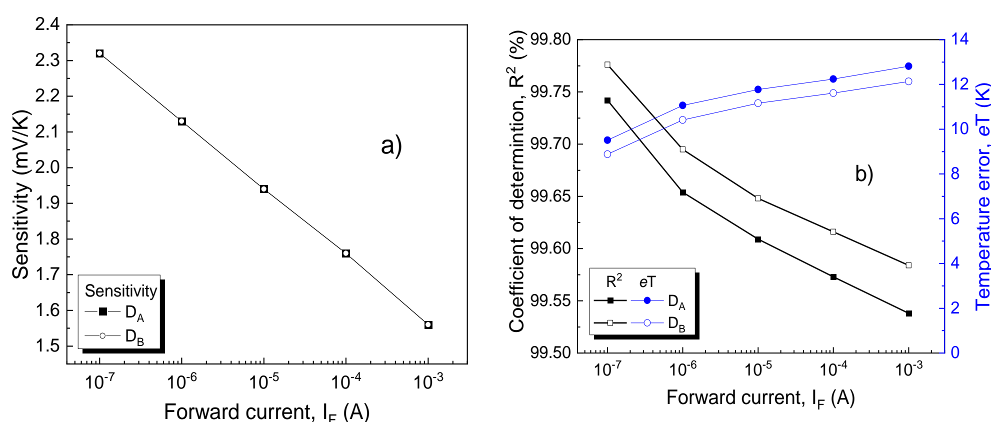

Figure 8. (**a**) Sensitivity, (**b**) coefficients of determination and average temperature error for both SiC Schottky diodes at different bias currents. For sensitivity, the absolute value was represented.

The sensitivities are nearly identical for D_A and D_B at all current levels, with a peak of 2.32 mV/K at 100 nA. Conversely, there are noticeable differences in linearity, favoring D_B. Even so, the highest value for R^2 is under 99.80%, below other reported results for such CTAT SiC-Schottky diode sensing elements [24,56]. These results confirm that extending the operation range to include both cryogenic and high-temperature levels, naturally impacts linearity (because of innate V_F variation, and contact inhomogeneity, as stated in Section 2.1).

Temperature-sensing performances were also evaluated for differential setups corresponding to the DDDC approach. Thus, Figure 9 presents the temperature variation of both voltage differentiation possibilities ($D_A \equiv D_h$, when $\Delta V_{F,AB} = V_{F,A} - V_{F,B}$ and $D_B \equiv D_h$, when $\Delta V_{F,BA} = V_{F,B} - V_{F,A}$) at several bias current ratios. A PTAT variation is observed. In this case, temperature-sensitive electrical behavior could only be achieved in the 100–700 K interval.

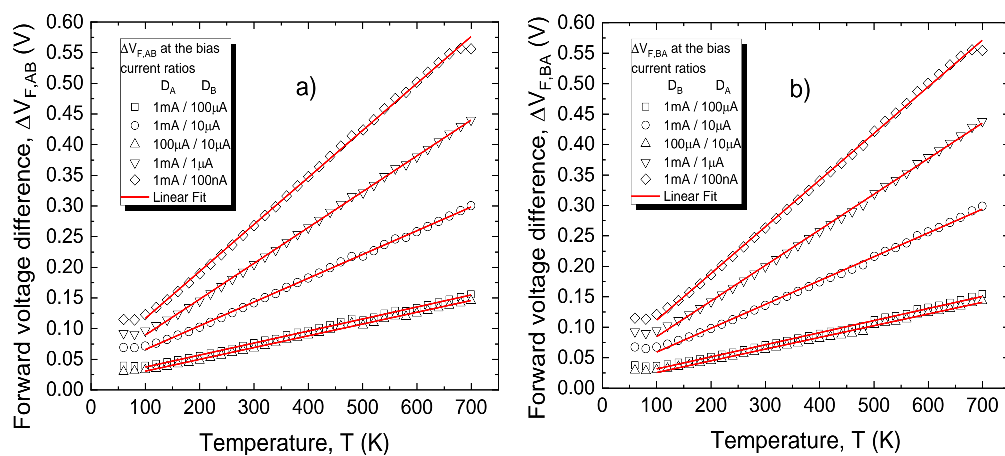

Figure 9. (**a**) $\Delta V_{F,AB}$ and (**b**) $\Delta V_{F,BA}$ with temperature, for different bias current ratios.

A linear regression process was also performed on the characteristics in Figure 9 in order to determine the sensitivity, linearity, and temperature error for the two DDDC configurations, with results plotted in Figure 10, for each current ratio.

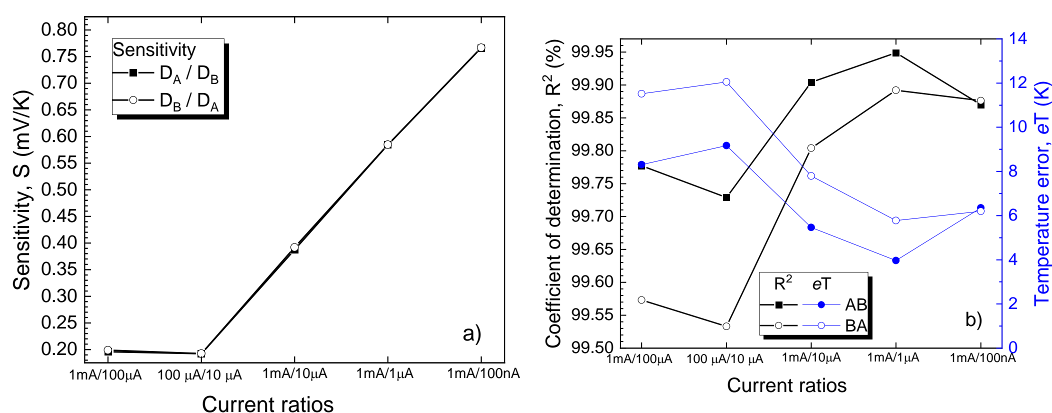

Figure 10. Sensitivity, coefficient of determination, and temperature error vs. diode current ratios for both differential configurations.

Sensitivity values increase with current ratio and are nearly identical between the $D_A \equiv D_h$ and $D_B \equiv D_h$ cases. The maximum obtained was approx. 0.77 mV/K for the 1 mA/100 nA bias current ratio. On the other hand, linearity is affected by topology, with a peak $R^2 \cong 99.95$ % achieved for the $D_A \equiv D_h$ setup, at a bias ratio of 1 mA/1 µA. This

result, together with a temperature error roughly three times lower, represent significant improvements over the CTAT variant (Figure 8b).

Overcoming the sensitivity loss of the DDDC approach can be achieved by using the circuit presented in Section 2.3. Investigations were carried out for the best-performing $D_A \equiv D_h$ configuration. In order to obtain the voltage-temperature dependence for the entire system, comprising both dual-diode sensing element and readout circuit, V_O as a function of input voltage difference was first simulated. P_1 (Figure 2) was set to 910 Ω, resulting in a gain of approx. 24 (Equation (5)). The obtained transfer characteristics were composed with the data in Figure 9b for the 1 mA/100 µA and 1 mA/1 µA bias currents. The simulations were repeated for a higher gain of 76 (P_1 set to 270 Ω) and again composed with the Figure 9b data. The resulting V_O (T) dependences are plotted in Figure 11, with sensing performances given in Table 2.

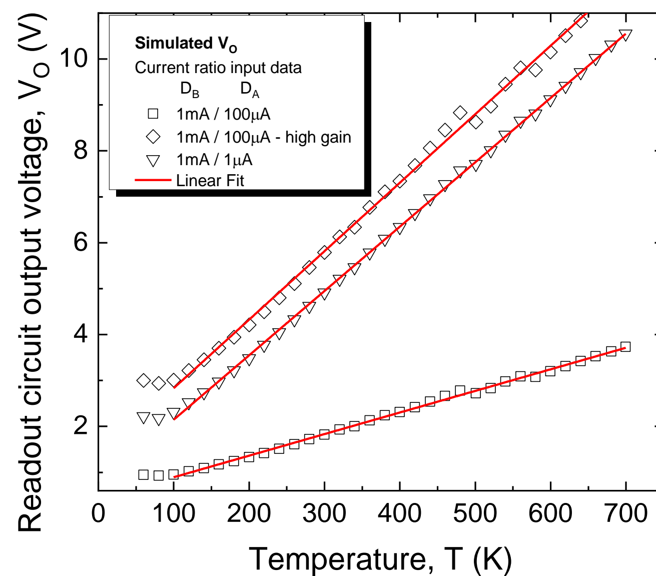

Figure 11. Simulated output voltage temperature dependence for the sensor system (dual-diode sensing element and readout circuit).

Table 2. Sensor system performances.

Bias Current Setup		Gain	S [mV/K]	$R^{2.5}$ [%]	Mean Squared Error [%]
$D_A \equiv D_h$	$D_B \equiv D_l$				
1 mA	100 µA	24	4.7	99.79	0.15
1 mA	100 µA	76	14.91	99.78	1.54
1 mA	1 µA	24	14.01	99.95	0.3

In all cases, adding the readout circuit significantly increases sensitivity, while keeping R^2 virtually unchanged. Compared to the CTAT variant, using a gain of 24 is sufficient in order to match and even exceed sensitivity performances, without affecting linearity. Increasing the readout circuit's gain further can compensate for S differences between bias current ratios; however, the mean squared error increases considerably (Table 2). Hence, only for the 1 mA/100 µA ratio, the gain could be increased to 76, which ensures maximum output swing for the readout circuit, while still maintaining linearity. The 1 mA/100 µA scenario was selected due to practical considerations. While it is obvious that the overall top results are attained for the 1 mA/1 µA case, obtaining accurate matching between such high-ratio current sources would notably increase the complexity and cost of the *I:nI Bias* block (Figure 2).

Sensing performances are summarized, alongside results obtained in recent papers, in Table 3. For a clear comparison, the sensing techniques are categorized separately.

Sensitivity and linearity values are similar between considered contributions, with this work covering over double the working temperature interval.

Table 3. Sensor system performance comparison.

	This Work	[39]	[46]	[55]
Sensing topology	Single SBD (CTAT)/Differential (PTAT)	Differential (PTAT)	Differential SBD/JBS (PTAT)	Single SBD (CTAT)
Temperature range	60–700 K (CTAT) 100–700 K (PTAT)	147–400 K	298–573 K	233–473 K
Sensitivity	2.32 mV/K (Single) 0.77 mV/K (Differential) 14.91 mV/K (Differential + Readout)	0.307 mV/K	4.32 mV/K (JBS) 2.85 mV/K (SBD)	3.425 mV/K
R^2	99.8% (Single) 99.95% (Differential)	99.93%	99.96%	99.96%

4. Conclusions

This paper presented a dual-diode structure suitable for thermal sensing over very wide intervals, from cryogenic to high-temperature. It comprises two SiC-Schottky diodes with matched contact areas and symmetrical layout, placed in close proximity. These devices have nearly identical forward current-voltage characteristics, making them suitable for differential measurements. A highly uniform Schottky contact, covered with Ni_2Si, was observed by XRD analysis on fabricated samples. Forward I-V-T measurements in the 60–700 K range evinced slight inhomogeneity. Thus, our p-diode technique was used to model the electrical behavior over the entire temperature domain, the largest reported so far. Two parallel diodes were sufficient in order to account for the majoritarian current at temperatures above 200 K. An additional two diodes were necessary for fitting lower temperature curves, at low-bias. The series resistance and effective surface of each parallel diode were taken into account in the model. Due to the large values obtained for these effective areas, the "pinch-off" effect was negligible, even at cryogenic temperatures.

The modeled dual-diodes proved suitable for CTAT and PTAT sensors over at least the 100–700 K range. For the CTAT variant, a high sensitivity was obtained (2.32 mV/K), with satisfactory linearity (R^2 upwards of 99.80%) down to 60 K. Significantly better linearity was observed for the PTAT differential version, with R^2 reaching 99.95%. In this case, the low sensitivity was overcome by using a high-performing, low-cost readout circuit. Simulations demonstrated sensitivities up to 14.91 mV/K, without affecting linearity.

Author Contributions: Conceptualization, R.P., G.B. and G.P.; methodology, G.B.; software, G.P.; formal analysis, F.D., G.B., M.S. and G.P.; investigation, R.P. and C.R.; resources, R.P., P.G. and F.D.; writing—original draft preparation, R.P., G.P. and F.D.; writing—review and editing, G.B., C.R., P.G., M.S. and A.T.; visualization, R.P., G.P., G.B., F.D., P.G. and A.T.; supervision, G.B. and F.D.; project administration, R.P. and G.P. All authors have read and agreed to the published version of the manuscript.

Funding: This work was supported in part by the PN-III-P2-2.1-PED-2019 Romanian Project under Contract SiC-HITs 275PED/2020, and in part by SiC-MOS under Project PN-III-P1-1.1-PD-2019-0924. Additionally, the article has benefitted from the support of the Operational Programme Human Capital of the Ministry of European Funds through the Financial Agreement under Grant 51675/09.07.2019, SMIS Code 125125.

Institutional Review Board Statement: Not applicable.

Informed Consent Statement: Not applicable.

Data Availability Statement: Not applicable.

Acknowledgments: The authors thank P. Varasteanu for schematic view of the test structures (Figure 1a).

Conflicts of Interest: The authors declare no conflict of interest.

References

1. Madhusoodhanan, S.; Koukourinkova, S.; White, T.; Chen, Z.; Zhao, Y.; Ware, M.E. Highly linear temperature sensor using GaN-on-SiC heterojunction diode for Harsh environment applications. In Proceedings of the 2016 IEEE 4th Workshop on Wide Bandgap Power Devices and Applications, Fayetteville, AR, USA, 7–9 November 2016; pp. 171–175. [CrossRef]
2. Kim, M.K.; Yoon, S.W. Miniature Piezoelectric Sensor for In-Situ Temperature Monitoring of Silicon and Silicon Carbide Power Modules Operating at High Temperature. *IEEE Trans. Ind. Appl.* **2018**, *54*, 1614–1621. [CrossRef]
3. Yakaboylu, G.A.; Pillai, R.C.; Sabolsky, K.; Sabolsky, E.M. Fabrication and thermoelectric characterization of transition metal silicide-based composite thermocouples. *Sensors* **2018**, *18*, 3759. [CrossRef] [PubMed]
4. Cui, J.; Liu, H.; Li, X.; Jiang, S.; Zhang, B.; Song, Y.; Zhang, W. Fabrication and characterization of nickel thin film as resistance temperature detector. *Vacuum* **2020**, *176*, 109288. [CrossRef]
5. Turkani, V.S.; Maddipatla, D.; Narakathu, B.B.; Altay, B.N.; Fleming, D.; Bazuin, B.J.; Atashbar, M.Z. A Screen-Printed Nickel Based Resistance Temperature Detector (RTD) on Thin Ceramic Substrate. In Proceedings of the 2020 IEEE International Conference on Electro Information Technology, Chicago, IL, USA, 31 July–1 August 2020; pp. 577–580. [CrossRef]
6. Park, S.; Byun, S. A 0.026 mm2 time domain cmos temperature sensor with simple current source. *Micromachines* **2020**, *11*, 899. [CrossRef] [PubMed]
7. Li, J.; Lin, Y.; Ning, N.; Yu, Q. A +0.44 °C/−0.4 °C Inaccuracy Temperature Sensor With Multi-Threshold MOSFET-Based Sensing Element and CMOS Thyristor-Based VCO. *IEEE Trans. Circuits Syst.* **2020**. [CrossRef]
8. Draghici, F.; Brezeanu, G.; Pristavu, G.; Pascu, R.; Badila, M.; Pribeanu, A.; Ceuca, E. 400 °C Sensor Based on Ni/4H-SiC Schottky Diode for Reliable Temperature Monitoring in Industrial Environments. *Sensors* **2019**, *19*, 2384. [CrossRef]
9. Pascu, R.; Craciunoiu, F.; Kusko, M. A promising technology of Schottky diode based on 4H-SiC for high temperature application. In Proceedings of the 2013 9th Conference on Ph.D. Research in Microelectronics and Electronics (PRIME), Villach, Austria, 24–27 June 2013; pp. 297–300.
10. Pascu, R.; Draghici, F.; Badila, M.; Craciunoiu, F.; Brezeanu, G.; Dinescu, A.; Rusu, I. High temperature sensor based on SiC Schottky diodes with undoped oxide ramp termination. In Proceedings of the International Semiconductor Conference, Sinaia, Romania, 17–19 October 2011; Volume 2, pp. 379–382.
11. Rahali, A.; Ouremchi, M.; Elboutahiri, A.; Elkhadiri, K.; Tahiri, A.; Qjidaa, H. Design of a Temperature Sensor with 0 °C to 120 °C Sensing Range for Li-Ion Battery Charger in 180 nm CMOS Technology. In Proceedings of the 2019 7th Mediterranean Congress of Telecommunications, Fès, Morocco, 24–25 October 2019; pp. 4–7. [CrossRef]
12. Megherbi, M.L.; Pezzimenti, F.; Dehimi, L.; Saadoune, M.A.; Della Corte, F.G. Analysis of trapping effects on the forward current-voltage characteristics of al-implanted 4H-SiC p-i-n Diodes. *IEEE Trans. Electron Devices* **2018**, *65*, 3371–3378. [CrossRef]
13. Bencherif, H.; Dehimi, L.; Pezzimenti, F.; Corte, F.G.D. Temperature and SiO2/4H-SiC interface trap effects on the electrical characteristics of low breakdown voltage MOSFETs. *Appl. Phys. A Mater. Sci. Process.* **2019**, *125*, 1–10. [CrossRef]
14. Fiorenza, P.; Giannazzo, F.; Cascino, S.; Saggio, M.; Roccaforte, F. Identification of two trapping mechanisms responsible of the threshold voltage variation in SiO2/4H-SiC MOSFETs. *Appl. Phys. Lett.* **2020**, *117*, 103502. [CrossRef]
15. Fiorenza, P.; Alessandrino, M.; Carbone, B.; Di Martino, C.; Russo, A.; Saggio, M.; Venuto, C.; Zanetti, E.; Giannazzo, F.; Roccaforte, F. Understanding the role of threading dislocations on 4H-SiC MOSFET breakdown under high temperature reverse bias stress. *Nanotechnology* **2020**, *31*, 125203. [CrossRef]
16. Kimoto, T.; Watanabe, H. Defect engineering in SiC technology for high-voltage power devices. *Appl. Phys. Express* **2020**, *13*, 120101. [CrossRef]
17. Pascu, R.; Pristavu, G.; Craciunoiu, F.; Badila, M.; Kusko, M.; Brezeanu, G.; Neamtu, J.; Gavrila, R. POCl3 annealing effect on the flat band voltage instabilities for a SiC based MOS capacitor at high temperature. *Rom. J. Inf. Sci. Technol.* **2014**, *17*, 340–352.
18. Pascu, R.; Craciunoiu, F.; Pristavu, G.; Brezeanu, G.; Kusko, M. Oxide trap states versus gas sensing in SiC-MOS capacitors–The effect of N- and P- based post oxidation processes. *Sens. Actuators B Chem.* **2017**, *245*, 911–922. [CrossRef]
19. Matthus, C.D.; Erlbacher, T.; Schöfer, B.; Bauer, A.J.; Frey, L. Implementation of 4H-SiC PiN-diodes as nearly linear temperature sensors up to 800 K towards SiC multi-sensor integration. *Mater. Sci. Forum* **2017**, *897 MSF*, 618–621. [CrossRef]
20. Sakakima, H.; Goryu, A.; Kano, A.; Hatano, A.; Hirohata, K.; Izumi, S. Modeling the effect of mechanical stress on bipolar degradation in 4H-SiC power devices. *J. Appl. Phys.* **2020**, *128*, 025701. [CrossRef]
21. Matthus, C.D.; Erlbacher, T.; Hess, A.; Bauer, A.J.; Frey, L. Advanced 4H-SiC p-i-n Diode as Highly Sensitive High-Temperature Sensor Up To 460 °C. *IEEE Trans. Electron Devices* **2017**, *64*, 3399–3404. [CrossRef]
22. Tanimoto, S.; Matsui, K. High junction temperature and low parasitic inductance power module technology for compact power conversion systems. *IEEE Trans. Electron Devices* **2015**, *62*, 258–269. [CrossRef]
23. Kaminski, N.; Rugen, S.; Hoffmann, F. Gaining Confidence–A Review of Silicon Carbide's Reliability Status. *IEEE Int. Reliab. Phys. Symp. Proc.* **2019**, 1–7. [CrossRef]
24. Pristavu, G.; Brezeanu, G.; Pascu, R.; Drăghici, F.; Bădilă, M. Characterization of non-uniform Ni/4H-SiC Schottky diodes for improved responsivity in high-temperature sensing. *Mater. Sci. Semicond. Process.* **2019**, *94*, 64–69. [CrossRef]
25. Brezeanu, G.; Pristavu, G.; Draghici, F.; Badila, M.; Pascu, R. Characterization technique for inhomogeneous 4H-SiC Schottky contacts: A practical model for high temperature behavior. *J. Appl. Phys.* **2017**, *122*, 084501. [CrossRef]

26. Pascu, R.; Kusko, M.; Craciunoiu, F.; Pristavu, G.; Brezeanu, G.; Badila, M.; Avramescu, V. A new 4H-SiC hydrogen sensor with oxide ramp termination. *Mater. Sci. Semicond. Process.* **2016**, *42*, 268–272. [CrossRef]
27. Della Corte, F.G.; Pangallo, G.; Rao, S.; Carotenuto, R.; Iero, D.; Merenda, M.; Pezzimenti, F. Use of 4H-SiC-based diodes as temperature sensors. In Proceedings of the 2019 International Semiconductor Conference, Sinaia, Romania, 9–11 October 2019; pp. 71–74. [CrossRef]
28. Rao, S.; Pangallo, G.; Pezzimenti, F.; Corte, F.G.D. High-Performance Temperature Sensor Based on 4H-SiC Schottky Diodes. *IEEE Electron Device Lett.* **2015**, *36*, 720–722. [CrossRef]
29. Kumar, V.; Maan, A.S.; Akhtar, J. Barrier height inhomogeneities induced anomaly in thermal sensitivity of Ni/4H-SiC Schottky diode temperature sensor. *J. Vac. Sci. Technol. B* **2014**, *32*, 041203. [CrossRef]
30. Pristavu, G.; Brezeanu, G.; Badila, M.; Draghici, F.; Pascu, R.; Craciunoiu, F.; Rusu, I.; Pribeanu, A. Barrier stability of Pt/4H-SiC schottky diodes used for high temperature sensing. In Proceedings of the Materials Science Forum (2016 European Conference on Silicon Carbide & Related Materials (ECSCRM), Halkidiki, Greece, 25–29 September 2016; Volume 897, pp. 606–609.
31. Pristavu, G.; Brezeanu, G.; Badila, M.; Draghici, F.; Pascu, R.; Craciunoiu, F.; Rusu, I.; Pribeanu, A. High Temperature Behavior Prediction Techniques for Non-Uniform Ni/SiC Schottky Diodes. *Mater. Sci. Forum* **2018**, *924*, 967–970. [CrossRef]
32. Tuy, T.Q.; Mojzes, I.; Szentpáli, B. The Dependence of Schottky Barrier Height of Metal-Semiconductor Contacts on the Ratio of Interfacial Area Occupied by Different Metal Components. *Mater. Sci. Forum* **1991**, *69*, 101–106. [CrossRef]
33. Tuy, T.Q.; Mojzes, I.; Szentpali, B. Dependence of Schottky barrier height on the ratio of different metal components. *Period. Polytech. Electr. Eng.* **1993**, *37*, 3–19.
34. Rang, T. *Modelling of Inhomogeneities of SiC Schottky Interfaces*; WIT Press: Ashurst Lodge, Ashurst, UK, 2001; pp. 3–15.
35. Roccaforte, F.; Giannazzo, F.; Alberti, A.; Spera, M.; Cannas, M.; Cora, I.; Pécz, B.; Iucolano, F.; Greco, G. Barrier inhomogeneity in vertical Schottky diodes on free standing gallium nitride. *Mater. Sci. Semicond. Process.* **2019**, *94*, 164–170. [CrossRef]
36. Bellone, S.; Di Benedetto, L.; Rubino, A. On the electrical behavior of V2O5/4H-SiC Schottky diodes. *J. Appl. Phys.* **2013**, *113*, 224503. [CrossRef]
37. Huang, L.; Qin, F.; Li, S.; Wang, D. Effects of surface properties on barrier height and barrier inhomogeneities of platinum contacts to n-type 4H-SiC. *Appl. Phys. Lett.* **2013**, *103*, 033520. [CrossRef]
38. Shivaraman, S.; Herman, L.H.; Rana, F.; Park, J.; Spencer, M.G. Schottky barrier inhomogeneities at the interface of few layer epitaxial graphene and silicon carbide. *Appl. Phys. Lett.* **2012**, *100*, 183112. [CrossRef]
39. Rao, S.; Pangallo, G.; Di Benedetto, L.; Rubino, A.; Licciardo, G.D.; Della Corte, F.G. A V2O5/4H-SiC Schottky diode-based PTAT sensor operating in a wide range of bias currents. *Sens. Actuators A Phys.* **2018**, *269*, 171–174. [CrossRef]
40. Brezeanu, G.; Pristavu, G.; Draghici, F.; Pascu, R.; Corte, F.D.; Rascuna, S. Enhanced Non-Uniformity Modeling of 4H-SiC Schottky Diode Characteristics Over Wide High Temperature and Forward Bias Ranges. *IEEE J. Electron Devices Soc.* **2020**, *8*, 1339–1344. [CrossRef]
41. Tung, R.T. Recent advances in Schottky barrier concepts. *Mater. Sci. Eng. R Rep.* **2001**, *35*, 1–138. [CrossRef]
42. Pristavu, G.; Brezeanu, G.; Badila, M.; Pascu, R.; Danila, M.; Godignon, P. A model to non-uniform Ni Schottky contact on SiC annealed at elevated temperatures. *Appl. Phys. Lett.* **2015**, *106*, 261605. [CrossRef]
43. Pascu, R.; Pristavu, G.; Brezeanu, G.; Draghici, F.; Badila, M.; Rusu, I.; Craciunoiu, F. Electrical Characterization of Ni-Silicide Schottky Contacts on SiC for High Performance Temperature Sensor. In *Materials Science Forum, Proceedings of the European Conference on Silicon Carbide & Related Materials (ECSCRM 2014), Grenoble, France, 21–25 September 2014*; Trans Tech Publications Ltd.: Stafa-Zurich, Switzerland; Volume 821–823, ISBN 9783038354789.
44. Gammon, P.M.; Pérez-Tomás, A.; Shah, V.A.; Vavasour, O.; Donchev, E.; Pang, J.S.; Myronov, M.; Fisher, C.A.; Jennings, M.R.; Leadley, D.R.; et al. Modelling the inhomogeneous SiC Schottky interface. *J. Appl. Phys.* **2013**, *114*, 223704. [CrossRef]
45. Roccaforte, F.; Giannazzo, F.; Raineri, V. Nanoscale transport properties at silicon carbide interfaces. *J. Phys. D Appl. Phys.* **2010**, *43*, 223001. [CrossRef]
46. Min, S.J.; Shin, M.C.; Nguyen, N.T.; Oh, J.M.; Koo, S.M. High-performance temperature sensors based on dual 4H-SiC JBS and SBD devices. *Materials* **2020**, *13*, 445. [CrossRef]
47. KERN, W. Cleaning solutions based on hydrogen peroxide for use in silicon semiconductor technology. *RCA Rev.* **1970**, *31*, 187–206.
48. Instruments, T. OP07x Precision Operational Amplifiers. Available online: https://www.ti.com/lit/ds/symlink/op07.pdf (accessed on 15 November 2020).
49. Instruments, T. REF200 Dual Current Source and Current Sink. Available online: https://www.ti.com/lit/ds/symlink/ref200.pdf (accessed on 15 November 2020).
50. La Via, F.; Roccaforte, F.; Raineri, V.; Musumeci, P.; Calcagno, L. Structural and electrical characterisation of titanium and nickel silicide contacts on silicon carbide. *Microelectron. Eng.* **2002**, *60*, 269–282. [CrossRef]
51. La Via, F.; Roccaforte, F.; Raineri, V.; Mauceri, M.; Ruggiero, A.; Musumeci, P.; Calcagno, L.; Castaldini, A.; Cavallini, A. Schottky-ohmic transition in nickel silicide/SiC-4H system: Is it really a solved problem? *Microelectron. Eng.* **2003**, *70*, 519–523. [CrossRef]
52. Kuchuk, A.; Kladko, V.; Guziewicz, M.; Piotrowska, A.; Minikayev, R.; Stonert, A.; Ratajczak, R. Fabrication and characterization of nickel silicide ohmic contacts to n-type 4H silicon carbide. *J. Phys. Conf. Ser.* **2008**, *100*, 042003. [CrossRef]
53. Williamson, G.K.; Hall, W.H. X-ray line broadening from filed aluminium and wolfram. *Acta Mater* **1953**, *1*, 22–31. [CrossRef]

54. Cheung, S.K.; Cheung, N.W. Extraction of Schottky diode parameters from forward current-voltage characteristics. *Appl. Phys. Lett.* **1986**, *49*, 85–87. [CrossRef]
55. Kumar, V.; Verma, J.; Maan, A.S.; Akhtar, J. Epitaxial 4H–SiC based Schottky diode temperature sensors in ultra-low current range. *Vacuum* **2020**, *182*, 109590. [CrossRef]
56. Rao, S.; Pangallo, G.; Di Benedetto, L.; Rubino, A.; Licciardo, G.D.; Corte, F.G.D. Divanadium Pentoxide/4H-silicon Carbide: A Schottky Contact for Highly Linear Temperature Sensors. *Procedia Eng.* **2016**, *168*, 1003–1006. [CrossRef]